Computational Scaffold Design for Bone Tissue Engineering: TPMS and Optimized Models

Eva Pavão Medeiros

evap.medeiros@gmail.com

Instituto Superior Técnico, Lisboa, Portugal

Abstract

Bone is a complex tissue of the human body with a wide variety of functions. Due to its importance, bone tissue engineering has been exploring new methods of facilitating the recovery of damaged bone, among which are scaffolds, a viable method and promising alternative to traditional methods. Scaffolds are artificially constructed porous support matrices which allow cell seeding, tissue regeneration, and provide support. These properties are dependent on the microstructure of the scaffold. TPMS geometries and optimized topologies are some of the better choices when it comes to designing these microstructures but their potentials are not yet fully understood. To compare these kinds of topologies, a set of TPMS geometries was chosen to compare with a series of optimized geometries created by a topology optimization tool. The optimized geometries were maximized for stiffness and/or permeability. The properties of all these topologies were calculated and compared. This comparison showed that while TPMS have some favorable properties, optimization tools can offer comparable or even better solutions of scaffold design, on top of being suitable for a wider variety of scenarios.

Key-words: Bone Tissue Engineering; Scaffolds; Triply Periodic Minimal Surfaces; Optimization; Permeability; Stiffness

1 Introduction

Scaffolds for bone tissue engineering (BTE) require high permeability, biocompatibility, bioactivity, degradability, and mechanical properties suited to the implantation site. Their internal geometry has a strong impact in these requirements, specifically permeability and mechanical properties. Triply periodic minimal surfaces (TPMS) have shown to be suitable in promoting tissue growth while providing the necessary support (Yoo, 2014). Optimized geometries focused on desired specifications are a promising alternative (Sturm et al., 2010) (Zhou & Li, 2008). However, it is still not fully known which method of geometry creation is the most suitable for BTE.

The aim of this work is to update an optimization tool used in Dias (2013) to create optimized geometries whose mechanical attributes and permeability are to be examined and compared to those of TPMS. With this, a further undertanding of the viability of optimized structures in BTE is sought.

2 Literature Review

3D printing and bioprinting allow for a precise control of the manufactured scaffold's geometry (Egan, 2019). Thus, careful consideration must be had when designing the geometry for the CAD models they use, as it will greatly impact mechanical properties, permeability, bioactivity, and biocompatibility (Zadpoor, 2015). The common approach used to create them is to design a unit cell and use it as a pattern for a lattice structure (Rosso et al., 2019) (Kladovasilakis et al., 2021) (Habib et al., 2016) (Egan et al., 2017). Depending on the desired properties of the scaffold as well as the materials and manufacturing method to be used, the unit cell can be a strut-like design, a TPMS, or an optimized geometry.

TPMS are surfaces defined by zero mean curvature and local area minimization (Torquato & Donev, 2004). They divide into continuous phases, making it possible to create structures with continuous and interconnected reinforcements. TPMS have been described showing enhanced mechanical properties and higher surface-to-volume ratio which greatly improves the bioactivity of the scaffold (Abueidda et al., 2019) (Yoo, 2014). Additionally, they have been able to obtain mechanical properties similar to that of bone and numerical simulation has considered them suited for further testing in BTE applications, but clinical verification of their viability is still lacking

(Castro, et al., 2020) (Castro et al., 2019) (Shi et al., 2018).

As an alternative, research has been done to use computer models to create optimized scaffold structures which have shown great potential for use in BTE scaffold design (Bendsøe & Sigmund, 2004) (Castilho et al., 2017) (Zhou & Li, 2008) (Dias et al., 2014).

3 Methodology

3.1 Homogenization Theory

The scaffolds in this work have a periodic microstructure of repeated cells, making the homogenization method an obvious and simple means to calculate their mechanical and permeability properties, following the method described by Guedes & Kikuchi (1990) and previously used by Dias (2013), Dias et al. (2014), and Coelho (2009).

To apply a homogenization approach, three assumptions must be made about the problem: periodicity, uniformity, and scale separation. In other words, the domain heterogeneities must be periodically distributed, so that all the corresponding domain properties are also periodic; the macroscopic fields must be uniform for all the microscopic representative volumes of the macroscopic domain; and the characteristic length scale of the microstructure size (d) should be much smaller than that of the macroscopic domain (D).

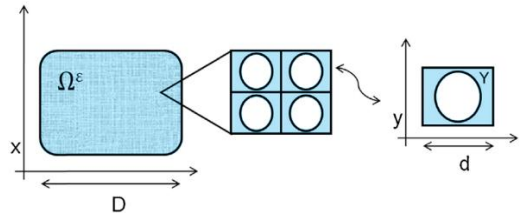

Figure 3.1: *Scheme of the homogenization method. Left: domain of the scaffold Ωε; center: detail of the domain; right: unit cell Y. d is the characteristic length scale of the microstructure size, represented by y; D is the characteristic length scale of the scaffold, represented by Y. Adapted from Dias et al. (2014).*

Following the work of Guedes & Kikuchi (1990), the elasticity and permeability coefficients are calculated through:

$$E^H_{ijkm} = \frac{1}{|Y|}\int_Y E_{pqrs}\left(\delta_{rk}\delta_{sm} - \frac{\partial \bar{\chi}^{km}_r}{\partial y_s}\right)\left(\delta_{pi}\delta_{qj} - \frac{\partial \bar{\chi}^{ij}_p}{\partial y_q}\right)dY \quad (3\text{-}1)$$

$$K^H_{im} = -\frac{1}{|Y|}\int_y K_{ij}\left(\delta_{jm} - \frac{\partial \chi^m}{\partial y_j}\right)dY \quad (3\text{-}2)$$

Here E^H are the homogenized elastic coefficients, the $\bar{\chi}$ functions represent deformation nodes for a unit cell subject to 6 unit average strains, the χ^m functions represent the microstructure pressure perturbations for a unit average pressure gradient in each direction m, and K^H_{im} is a matrix representing the homogenized coefficients of permeability.

3.2 Optimization Tool

The optimization tool used in this work is an updated and improved version of the one described by Dias (2013). Originally written in FORTRAN 77, it was converted to Fortran 90 to facilitate memory allocation and future alterations. Many of the user given inputs were altered, preventing redundancy, adding more control over the chosen problem, and removing the need to recompile the program whenever certain inputs needed to be changed. Outputs were made easier to read and identify.

This optimization obtains geometries for unit cells by solving topology optimization problems in which it must define whether there is material or not at each point of the microstructure domain. For this, the material density ρ is used as a variable field and its maximum (1) and minimum (0) values correspond to solid and void material, respectively.

While other mesh sizes can be used, for this work all cells were defined by 20x20x20 models of 8-node cuboid elements.

The relative permeability (FPerm) of a scaffold was then defined as the average of the homogenized coefficients on the main directions, and calculated by:

$$FPerm = \frac{K^H_{11} + K^H_{22} + K^H_{33}}{3} \quad (3\text{-}3)$$

FPerm is a relative value which can go from 0 (in the case of a completely solid cell) to 1 (when the cell is completely void).

The stiffness of a scaffold is then calculated by:

$$FElast = \frac{\varepsilon E^H \varepsilon}{2} \quad (3\text{-}4)$$

Where E^H are the homogenized elastic coefficients, and ε is a given strain field.

3.2.1 Problem Formulation

The density field describing the scaffold's microstructure will be the solution of the topology optimization problem described generally as:

$$\begin{aligned} &minimize \quad F_{obj} \\ &subject\ to \quad F_i(\rho) \leq F_i^*, \ i = 1, \dots, m \\ &0 \leq \rho \leq 1 \end{aligned} \tag{3-5}$$

Where F_{obj} is the objective function and F_i are the constraint functions. The solution of an optimization problem is based on the resolution of the necessary optimal conditions of Karush-Kuhn-Tucker (KKT) (Coelho, 2009). A finite element (FE) procedure was used to solve the elasticity and permeability homogenization problems for the cells. Additionally, the SIMP model is followed, meaning that the final geometry ideally only has densities of 0 or 1, as long as no failure to converge is met.

The method of moving asymptotes (MMA) was employed to solve the topology optimization problem itself (Svanberg, 1987), since it was shown to be very well adjusted to solving problems with a high number of design variables, which in this case are the density values for each element of the cell.

3.3 CFD Permeability

Computational fluid dynamics (CFD) through the software FLUENT ® ANSYS ® (Ansys Inc., Canonsburg, Pennsylvania, USA) was chosen as the alternate method to calculate scaffold permeability, following procedures used by Pires (2019) and Guerreiro et al. (2020).

3.4 TPMS geometries

The models for the TPMS topologies created for this work were designed computationally, using the program developed by Dinis et al. (2014).

For this work, nine TPMS topologies were used for comparisons: SP, SD, and SG, with porosities of approximately 60%, 70% and 80%, following previous work (Pires, 2019) (Dias, 2013) (Guerreiro et al., 2020). These TPMS geometries will in the rest of this work be referred to by their geometry and porosity.

4 Results and Discussion

4.1 Optimization attribute variability

The optimization tool was run for the multi-objective problem type, for VF values of 20, 30, and 40, for all initial solutions and for α values between 0.1 and 0.9. Not all of the resulting topologies met the VF requirements due to local solutions. Optimized structures were created under these criteria for strain fields ε=[1,1,1,0,0,0] and ε=[0,0,0,1,1,1], representing a triaxial normal strain field and a triaxial shear strain field, respectively.

It can be initially seen that some parameters were much more likely to lead to a converged solution than others. In **Table 4.1**, it can be seen that the initial solution d7 was more likely to lead to favorable converged solutions, whereas in **Table 4.2** the same can be said for d1 and d4. Additionally, there are more geometries with 60% porosity than of the other porosities. The amount of material at disposal with 60% porosity makes it more likely to obtain a mechanically sound structure, following the

***Table 3.1**: TPMS geometries used for comparison and their attributes.*

TPMS	*CFD (mm²)*	*FPerm*	*Exx*	*FElast ε=[1,1,1,0,0,0]*	*FElast ε=[0,0,0,1,1,1]*
SD80	5.513×10^{-4}	0.650	7.542×10^{-2}	2.106×10^{-1}	2.113×10^{-2}
SD70	3.169×10^{-4}	0.430	1.253×10^{-1}	3.666×10^{-1}	4.296×10^{-2}
SD60	2.059×10^{-4}	0.322	1.904×10^{-1}	5.650×10^{-1}	7.740×10^{-2}
SG80	8.827×10^{-4}	0.586	5.090×10^{-2}	1.789×10^{-1}	3.110×10^{-2}
SG70	5.054×10^{-4}	0.407	9.156×10^{-2}	3.171×10^{-1}	5.780×10^{-2}
SG60	3.342×10^{-4}	0.328	1.513×10^{-1}	4.996×10^{-1}	9.631×10^{-2}
SP80	6.528×10^{-4}	0.527	4.227×10^{-2}	2.733×10^{-1}	4.685×10^{-2}
SP70	4.571×10^{-4}	0.371	8.567×10^{-2}	4.397×10^{-1}	8.075×10^{-2}
SP60	2.068×10^{-4}	0.263	1.550×10^{-1}	6.480×10^{-1}	1.253×10^{-1}

requirements of F_{obj}. In addition, a lot of structures for high porosity values had "fluid pockets", as the optimization tool sought to reach the required VF by removing material from places where it wouldn't greatly affect mechanical properties.

Table 4.1: *Properties of optimized topologies created using the multi-objective problem for the given α values, initial solutions, VF, and for ε=[1,1,1, 0,0,0].*

Initial solution	α	VF (%)	Permeability	FPerm	Exx	FElast ε=[1,1,1,0,0,0]	FElast ε=[0,0,0,1,1,1]
d7	0.1	80	2.22×10^{-3}	0.61	7.97×10^{-2}	1.99×10^{-1}	1.87×10^{-2}
d7	0.1	70	8.78×10^{-4}	0.45	1.17×10^{-1}	3.72×10^{-1}	5.74×10^{-2}
d7	0.1	60	2.59×10^{-4}	0.23	1.49×10^{-1}	6.46×10^{-1}	1.20×10^{-1}
d7	0.2	80	2.33×10^{-3}	0.61	7.80×10^{-2}	1.95×10^{-1}	1.78×10^{-2}
d3	0.2	70	6.83×10^{-4}	0.26	8.78×10^{-2}	4.14×10^{-1}	6.93×10^{-2}
d7	0.2	70	5.04×10^{-4}	0.41	8.79×10^{-2}	4.14×10^{-1}	7.23×10^{-2}
d7	0.2	60	2.95×10^{-4}	0.30	1.56×10^{-1}	6.51×10^{-1}	1.21×10^{-1}
d7	0.3	80	2.68×10^{-3}	0.63	8.52×10^{-2}	1.92×10^{-1}	1.48×10^{-2}
d1	0.3	70	7.35×10^{-4}	0.45	1.06×10^{-1}	3.70×10^{-1}	5.84×10^{-2}
d7	0.3	70	5.64×10^{-4}	0.33	8.52×10^{-2}	4.02×10^{-1}	6.99×10^{-2}
d1	0.3	60	2.98×10^{-4}	0.24	1.51×10^{-1}	6.39×10^{-1}	1.18×10^{-1}
d3	0.3	60	3.31×10^{-4}	0.24	1.47×10^{-1}	6.32×10^{-1}	1.17×10^{-1}
d7	0.3	60	2.96×10^{-4}	0.24	1.47×10^{-1}	6.32×10^{-1}	1.18×10^{-1}
d7	0.4	80	3.21×10^{-3}	0.64	8.59×10^{-2}	1.88×10^{-1}	1.35×10^{-2}
d1	0.4	70	7.21×10^{-4}	0.34	8.81×10^{-2}	4.16×10^{-1}	7.08×10^{-2}
d7	0.4	70	5.53×10^{-4}	0.34	8.81×10^{-2}	4.16×10^{-1}	7.25×10^{-2}
d4	0.4	60	5.15×10^{-4}	0.37	1.49×10^{-1}	5.20×10^{-1}	1.01×10^{-1}
d7	0.4	60	3.30×10^{-4}	0.25	1.48×10^{-1}	6.26×10^{-1}	1.16×10^{-1}
d1	0.5	70	7.74×10^{-4}	0.45	1.07×10^{-1}	3.09×10^{-1}	3.57×10^{-2}
d7	0.5	70	5.53×10^{-4}	0.34	8.81×10^{-2}	4.16×10^{-1}	7.25×10^{-2}
d7	0.5	60	3.42×10^{-4}	0.34	1.48×10^{-1}	6.23×10^{-1}	1.14×10^{-1}
d7	0.6	80	2.52×10^{-3}	0.65	9.60×10^{-2}	1.75×10^{-1}	1.03×10^{-2}
d4	0.6	70	1.43×10^{-3}	0.48	1.14×10^{-1}	3.04×10^{-1}	5.06×10^{-2}
d7	0.6	70	1.22×10^{-3}	0.49	1.33×10^{-1}	3.37×10^{-1}	4.15×10^{-2}
d6	0.6	60	3.18×10^{-4}	0.32	1.54×10^{-1}	6.10×10^{-1}	1.11×10^{-1}
d7	0.6	60	3.76×10^{-4}	0.32	1.49×10^{-1}	6.22×10^{-1}	1.14×10^{-1}
d6	0.7	60	8.37×10^{-4}	0.37	2.12×10^{-1}	4.96×10^{-1}	7.19×10^{-2}

For the normal strain field, most of the optimized structures were shaped like SPs. The higher elastic modulus associated with these structures might have been the cause for this phenomenon (Maskery et al., 2018). For the shear strain field, the majority of the structures were, however, a series of diagonal pillars. These later ones would realistically not be possible to print, as there is nothing supporting their separate parts. However, because the optimization tool considers them as part of an infinitively periodical structure, the homogenized elasticity coefficients, especially in the directions of the strain field, are computed as generally on the same scale as those of the normal strain field geometries.

For most cases, optimized topologies can achieve the same parameters as TPMS, or higher values. For 80% and 70% porosity, the optimized structures obtained all have higher permeability than the TPMS.

SG60's permeability falls within the range of values from the optimized geometries, but these still achieve higher permeability values. The Young's modulus Exx of optimized topologies created for a deformation field ε=[0,0,0,1,1,1] is, as expected, much lower than that of the other topologies. For ε=[1,1,1,0,0,0], the Optimized structures once again show values higher or equal to those of TPMS.

Table 4.2: *Properties of optimized topologies created using the multi-objective problem for the given α values, initial solutions, VF, and for ε=[0,0,0,1,1,1].*

Initial solution	α	VF (%)	Permeability	FPerm	Exx	FElast ε=[1,1,1,0,0,0]	FElast ε=[0,0,0,1,1,1]
d1	0.2	80	3.72×10^{-3}	0.70	8.05×10^{-3}	1.33×10^{-1}	8.46×10^{-2}
d3	0.2	80	3.71×10^{-3}	0.70	8.05×10^{-3}	1.33×10^{-1}	8.49×10^{-2}
d7	0.2	80	2.02×10^{-3}	0.62	1.92×10^{-7}	6.31×10^{-7}	1.18×10^{-7}
d1	0.2	70	2.80×10^{-3}	0.59	1.83×10^{-2}	2.06×10^{-1}	1.19×10^{-1}
d4	0.2	70	1.21×10^{-3}	0.59	2.26×10^{-7}	7.38×10^{-7}	1.41×10^{-7}
d1	0.2	60	1.08×10^{-3}	0.48	3.51×10^{-2}	2.95×10^{-1}	1.54×10^{-1}
d4	0.2	60	6.23×10^{-4}	0.46	3.20×10^{-7}	9.95×10^{-7}	2.01×10^{-7}
d7	0.2	60	9.26×10^{-4}	0.41	2.94×10^{-2}	2.67×10^{-1}	1.43×10^{-1}
d4	0.4	60	6.27×10^{-4}	0.46	3.19×10^{-7}	9.93×10^{-7}	2.01×10^{-7}
d7	0.5	80	2.28×10^{-3}	0.54	4.91×10^{-3}	1.17×10^{-1}	6.16×10^{-3}
d4	0.5	60	6.15×10^{-4}	0.46	3.51×10^{-2}	9.99×10^{-7}	2.03×10^{-7}
d6	0.5	60	1.02×10^{-3}	0.42	3.12×10^{-2}	2.76×10^{-1}	1.48×10^{-1}

The same generalizations cannot be made for FElast values. Again, the optimized topologies created for ε=[0,0,0,1,1,1] underperform. The other optimized topologies have value ranges that encompass the TPMS's totally or partially, with SP70 and SD80 having a higher value, as well as the SD80. The optimized geometries made for ε=[0,0,0,1,1,1] show great variability of FElast values, including both higher and much lower values than the TPMS. Optimized geometries for ε=[1,1,1,0,0,0] show a range of FElast values encompassing most of the TPMS, but not reaching as high as the SP60 and SP70. For 80% porosity, all TPMS achieve higher FElast values than these optimized geometries.

While there are some specific cases in which Optimized geometries cannot replicate the combined attributes of TPMS, the wide choices of initial parameter values allow for wide variety of end results. This means that an Optimized geometry can be made to be better tailored to a problem than any TPMS at hand.

4.2 Optimizing TPMS geometries

The previously mentioned set of 9 TPMS was used as initial solutions in the optimization tool, with ε=[1,1,1,0,0,0]. From each of these TPMSs, four different geometries were created: two from the rigidity optimization problem and another two from the permeability optimization problem. For each of these sets of twos, one of the geometries was created utilizing solely the constraint function on the VF, while the other used the two constraint functions of the given problem type.

The objective of these tests was to see if the given TPMS could have their permeability properties Optimized, while maintaining the same porosity and elastic properties, or if they could have their elastic properties Optimized, while maintaining the same porosity and permeability properties.

The properties of the resulting geometries were very similar or equal to those of the TPMS. As seen in **Table 4.3**, the variations in values are very small, with every attribute showing a maximum deviation an order of magnitude smaller than the original value, with the exception of porosity, which has a maximum deviation of 3%.

These optimized geometries only suffered minor alterations, which explains why the attributes retained very similar values.

Table 4.3: *Maximum deviations of values between TPMS and the optimized structures which used them as initial solutions.*

TPMS	Porosity (%)	Permeability (CFD, mm²)	FPerm	Exx	Felast ε=[1,1,1,0,0,0]
SD60	0.750	0.000	2.768×10^{-7}	1.868×10^{-3}	5.316×10^{-3}
SD70	0.000	0.000	7.767×10^{-3}	0.000	0.000
SD80	0.600	1.610×10^{-5}	1.858×10^{-8}	2.316×10^{-3}	6.781×10^{-3}
SG60	0.000	0.000	3.612×10^{-3}	0.000	3.000×10^{-8}
SG70	0.000	0.000	1.399×10^{-2}	0.000	3.000×10^{-8}
SG80	0.225	2.426×10^{-5}	1.679×10^{-2}	3.690×10^{-5}	3.403×10^{-3}
SP60	0.000	0.000	6.386×10^{-4}	0.000	1.500×10^{-7}
SP70	0.000	0.000	4.640×10^{-6}	0.000	1.000×10^{-8}
SP80	3.000	0.000	4.005×10^{-8}	7.767×10^{-3}	4.073×10^{-2}
Maximum deviation	3.000	2.426×10^{-5}	1.679×10^{-2}	7.767×10^{-3}	4.073×10^{-2}

Because the F_{obj} to be minimized is not well-behaved (that is, it does not have a single global minimum, but instead has multiple local minimums in addition to the global one), the results given by it are local best solutions. Given that the initial solutions already fulfilled the constraint function requirements, the fact that the objective function could not be further minimized implies that the TPMS structures are already considered a local best.

4.3 Replication of TPMS properties

For this section the goal was to create optimized structures with some of the same properties as TPMS. To do this, two sets of nine optimized structures were made, one under the rigidity optimization problem, and the other under the permeability optimization problem. For each set, the properties of the TPMS were used in the constraint functions. All structures used the same initial solution d7 and ε=[1,1,1,0,0,0].

Due to the nature of the optimization tool's problem types, it was not always possible to meet both constraint function attribute values, or even optimize the objective function attribute above that of the respective TPMS. The SG80 case under permeability optimization was not considered due to consistently failing to meet constraint function values.

Comparing the values of **Table 3.1** with those of **Table 4.4** and **Table 4.5**, a common factor that can be noted is that the structures optimized for permeability will often show higher FElast values than the ones optimized for rigidity. This is because both constraint functions of the later problem type lead to higher porosity and FPerm values, making it so that the highest FElast value achievable can become lower. The reverse is observed in the structures optimized for permeability, where their FPerm values are often lower due to the constraint functions pushing for a lower porosity and higher FElast values.

Taking a particular case, the geometry for SG70 in **Table 4.4** keeps almost the exact porosity required but reaches a higher FPerm and thus higher permeability, with a lower FElast. In another example, that of the geometry for SD60 in **Table 4.5**, it can be seen a case where some porosity was sacrificed but all the other attributes managed to obtain higher values than the respective TPMS. While some trends can be seen in these tables, such as the increment of FElast as the porosity decreases for each set of optimized geometries replicating properties of a type of TPMS, vast differences in shape can alter some of these trends.

Overall, it cannot be said that the optimization tool in its current state can easily create a topology with the same porosity and FElast (or FPerm) as a pre-existing structure, but with a higher FPerm (or FElast).

***Table 4.4**: Attributes of nine geometries created from the same initial solution under the rigidity optimization problem. Constraint functions used the VF and FPerm of the respective TPMS.*

TPMS	Porosity (%)	Permeability (CFD, mm²)	FPerm	Exx	FElast ε=[1,1,1,0,0,0]
SD60	62.40	1.10×10^{-3}	0.32	1.32×10^{-1}	5.44×10^{-1}
SD70	70.20	1.46×10^{-3}	0.54	1.49×10^{-1}	2.86×10^{-1}
SD80	89.60	4.47×10^{-3}	0.76	4.32×10^{-2}	7.32×10^{-2}
SG60	64.80	1.20×10^{-3}	0.44	1.84×10^{-1}	3.66×10^{-1}
SG70	69.90	1.46×10^{-3}	0.55	1.52×10^{-1}	2.93×10^{-1}
SG80	79.80	2.74×10^{-3}	0.65	8.11×10^{-2}	1.83×10^{-1}
SP60	59.60	3.30×10^{-4}	0.26	1.51×10^{-1}	6.33×10^{-1}
SP70	70.40	6.85×10^{-4}	0.37	9.74×10^{-2}	3.80×10^{-1}
SP80	79.80	2.52×10^{-3}	0.63	7.73×10^{-2}	1.89×10^{-1}

***Table 4.5**: Attributes of 8 geometries created from the same initial solution under the permeability optimization problem. Constraint functions used the VF and FElast of the respective TPMS.*

TPMS	Porosity (%)	Permeability (CFD, mm²)	FPerm	Exx	Felast ε=[1,1,1,0,0,0]
SD60	53.70	8.34×10^{-4}	0.35	2.81×10^{-1}	6.27×10^{-1}
SD70	62.70	2.54×10^{-4}	0.44	1.75×10^{-1}	4.18×10^{-1}
SD80	73.30	1.41×10^{-3}	0.56	1.31×10^{-1}	2.53×10^{-1}
SG60	54.30	8.76×10^{-4}	0.36	2.74×10^{-1}	6.04×10^{-1}
SG70	64.00	1.13×10^{-3}	0.43	1.99×10^{-1}	4.08×10^{-1}
SP60	52.80	5.90×10^{-4}	0.32	2.92×10^{-1}	6.56×10^{-1}
SP70	68.30	4.98×10^{-4}	0.41	9.39×10^{-2}	4.47×10^{-1}
SP80	71.20	2.21×10^{-3}	0.55	1.44×10^{-1}	2.77×10^{-1}

5 Conclusions and Future Work

The objective of this work was to update a preexisting optimization tool and use it to gain a better understanding of the properties of optimized topologies, in order to determine if they are a viable option, or even a better option than the more widely used TPMS structures. In this section, the results obtained during this work are reviewed, and ideas for future research are discussed.

5.1 Conclusions

To explore the properties of optimized topologies, a topology optimization tool previously used in Dias (2013) and Dias et al. (2014) had its code updated to Fortran 90, and was changed to allow a series of problem types at the users choice. The optimized geometries created were then compared with TPMS geometries.

To explore the range of values that the attributes of optimized topologies can obtain, a series of them were created using the multi-objective problem, for all the initial solutions and porosities used. When comparing attribute values, it could be seen that optimized geometries achieved much wider range of permeability and elasticity values than the TPMS. For the same porosities, optimized topologies could be made to obtain both permeabilities and elasticity values. It is of note that for triaxial normal strain fields, the optimized topologies resulted in SP-like geometries, despite none of the initial solutions being similar to that shape.

When using the chosen TPMS geometries as initial solutions for the optimization tool, it was found that the resulting optimized geometry did not improve upon the original, presenting little to no changes. Given that the objective function to be minimized, which is used to define the problem in the optimization tool, has multiple local minimums in additional to the global minimum, the TPMS structures can be one of these local minimums or local solutions.

Creating optimized geometries from the same initial solution d7 using permeability optimization with a constraint on elasticity or elasticity optimization with a constraint on permeability to obtain the same attributes as the TPMS geometries yielded a series of geometries with attributes in the same scale as the TPMS ones. Not all geometries were optimized, and those who were tended to show changes in porosity in order to obtain the higher permeability or elasticity. Overall, optimized topologies were shown to have more specificity and versatility, as they can be created for specific load scenarios and permeability or stiffness requirements. Topology optimization tools such as the one used in this work can be used for a variety of materials and be edited to use other problem types, such as mechanobiology-based optimization algorithms or steady-state Navier–Stokes flow optimization (Boccaccio et al., 2018) (Zhou & Li, 2008).

With this versatility in mind, and given that optimized topologies were shown in this work to also be able to obtain permeability and mechanical properties on par with TPMS geometries, it can be concluded that optimization has a lot of potential not only for scaffold design in BTE but in other areas of tissue engineering as well.

5.2 Future Work

The results obtained throughout this work showcase the importance of studying the capabilities of topology optimization tools and their possible application in BTE. This has given rise to further work regarding not only the optimization tool itself but also the use of optimized topologies.

One of the major drawbacks of the optimization tool used was the limitations in problem construction. In addition to maximizing permeability, elasticity, or a mix of both, other parameters relevant for scaffold construction should be explored, such as surface area, or wall shear stress, which relate to the bioactivity and degradability of the scaffold. For example, it might prove useful to maximize a geometry's mechanical properties to ensure it supports the loads at the implantation site, while placing a constraint on wall shear stress, in order to prevent too-slow degradation.

In addition, the optimization tool did not take into account whether the optimized structure could be printed and safely implanted. For a triaxial shear strain field, the vast majority of the optimal geometries were composed of separate pieces of material. These geometries could only realistically hold shape if printed with solid walls, which would severely affect the scaffold's permeability. In a triaxial normal strain field, this was a much more uncommon phenomenon (only present when elasticity was not taken into consideration). However, structures with "fluid pockets", that is, structures with isolated pores with no connectivity, would be occasionally produced, more commonly for the highest porosity used: 80%. While these do not produce a great impact on the mechanical properties and aid in meeting VF requirements, these pores could end up filled with toxic materials during the printing process. Following scaffold degradation, these materials are released, making it unsuitable for use in tissue engineering. In the future, it would be ideal for the optimization tool to identify and avoid outputting geometries having such incompatibilities with the manufacturing process. Further research on the applicability of optimized topologies for BTE is also needed. Ultimately, it is through ex-vivo and in-vivo testing that we might better understand if optimized topologies do meet the requirements of scaffolds in BTE.

6 Bibliography

Abueidda, D., Elhebeary, M., Shiang, C. S. (Andrew), Pang, S., Abu Al-Rub, R. K., & Jasiuk, I. M. (2019). *Mechanical properties of 3D printed polymeric Gyroid cellular structures: Experimental and finite element study.* Materials and Design, 165, 107597.

Bendsøe, M., & Sigmund, O. (2004). *Topology Optimization - Theory, Methods, and Applications.* Springer Berlin Heidelberg.

Boccaccio, A., Fiorentino, M., Uva, A. E., Laghetti, L. N., & Monno, G. (2018).

Rhombicuboctahedron unit cell based scaffolds for bone regeneration: geometry optimization with a mechanobiology – driven algorithm. Materials Science and Engineering C, 83, pp. 51–66.

Castilho, M., Rodrigues, J., Vorndran, E., Gbureck, U., Quental, C., Folgado, J., & Fernandes, P. R. (2017). *Computational design and fabrication of a novel bioresorbable cage for tibial tuberosity advancement application.* Journal of the Mechanical Behavior of Biomedical Materials, 65, pp. 344–355.

Castro, , A., Santos, J., Pires, T., & Fernandes, P. R. (2020). *Micromechanical Behavior of TPMS Scaffolds for Bone Tissue Engineering.* Macromolecular Materials and Engineering, 2000487, pp. 1–10.

Castro, A., Ruben, R. B., Gonçalves, S. B., Pinheiro, J., Guedes, J. M., & Fernandes, P. R. (2019). *Numerical and experimental evaluation of TPMS Gyroid scaffolds for bone tissue engineering.* Computer Methods in Biomechanics and Biomedical Engineering, 22(6), pp. 567–573.

Coelho, P. (2009). *Modelos hierárquicos para a análise e síntese de estruturas e materiais com aplicações à remodelação óssea.* [Doctoral dissertation, Faculdade de Ciências e Tecnologia - Universidade Nova de Lisboa].

Dias, M. (2013). *Scaffold Design for Bone Tissue Engineering.* [Doctoral dissertation, Instituto Superior Técnico].

Dias, M., Fernandes, P. R., Guedes, J. M., & Hollister, S. J. (2012). *Permeability analysis of scaffolds for bone tissue engineering.* Journal of Biomechanics, 45(6), pp. 938–944.

Dias, M., Guedes, J. M., Flanagan, C. L., Hollister, S. J., & Fernandes, P. R. (2014). *Optimization of scaffold design for bone tissue engineering: A computational and experimental study.* Medical Engineering and Physics, 36(4), pp. 448–457.

Dinis, J., Morais, T. F., Amorim, P. H. J., Ruben, R. B., Almeida, H. A., Inforçati, P. N., . . . Silva, J. V. L. (2014). *Open Source Software for the Automatic Design of Scaffold Structures for Tissue Engineering Applications.* Procedia Technology, 16(December), pp. 1542–1547.

Egan, P. (2019). *Integrated design approaches for 3D printed tissue scaffolds: Review and outlook.* Materials, 12(15), 2355.

Egan, P., Gonella, V. C., Engensperger, M., Ferguson, S. J., & Shea, K. (2017). *Computationally designed lattices with tuned properties for tissue engineering using 3D printing.* PLoS ONE, 12(8), pp. 1–20.

Guedes, J., & Kikuchi, N. (1990). *Preprocessing and postprocessing for materials based on the homogenization method with adaptive finite element methods.* Computer Methods in Applied Mechanics and Engineering, 83(2), pp. 143–198.

Guerreiro, R., Pires, T., Guedes, J. M., Fernandes, P., & Castro, A. (2020). *On*

the Tortuosity of TPMS Scaffolds for Tissue Engineering. Symmetry, 12(4), pp. 596.

Habib, F., Nikzad, M., Masood, S. H., & Saifullah, A. B. M. (2016). *Design and development of scaffolds for tissue engineering using three-dimensional printing for bio-based applications.* 3D Printing and Additive Manufacturing, 3(2), pp. 119–127.

Kladovasilakis, N., Tsongas, K., & Tzetzis, D. (2021). *Mechanical and fea-assisted characterization of fused filament fabricated triply periodic minimal surface structures.* Journal of Composites Science, 5(2):58.

Maskery, I., Sturm, L., Aremu, A. O., Panesar, A., Williams, C. B., Tuck, C. J., . . . Hague, R. J. M. (2018). *Insights into the mechanical properties of several triply periodic minimal surface lattice structures made by polymer additive manufacturing.* Polymer, 152, pp. 62–71.

Pires, T. (2019). *Computational fluid dynamics simulation of TPMS scaffolds for bone tissue engineering.* [Masters' thesis, Instituto Superior Técnico].

Rosso, S., Savio, G., Uriati, F., Meneghello, R., & Concheri, G. (2019). *Optimization approaches in design for additive manufacturing.* Proceedings of the International Conference on Engineering Design, ICED, 2019-August(AUGUST), pp. 809–818.

Shi, J., Zhu, L., Li, L., Li, Z., Yang, J., & Wang, X. (2018). *A TPMS-based method for modeling porous scaffolds for bionic bone tissue engineering.* Scientific Reports, 8(1) pp. 7395.

Sturm, S., Zhou, S., Mai, Y. W., & Li, Q. (2010). *On stiffness of scaffolds for bone tissue engineering-a numerical study.* Journal of Biomechanics, 43(9), pp. 1738–1744.

Svanberg, K. (1987). *The Method of Moving Asymptotes -A New Method for Structural Optimization.* International Journal for Numerical Methods in Engineering, 24, pp. 359–373.

Torquato, S., & Donev, A. (2004). *Minimal surfaces and multifunctionality.* Proceedings of the Royal Society A: Mathematical, Physical and Engineering Sciences, 460(2047), pp. 1849–1856.

Yoo, D.-J. (2014). *Advanced Porous Scaffold Design using Multi-Void Triply Periodic Minimal Surface Models with High Surface Area to Volume Ratios.* International Journal of Precision Engineering and Manufacturing, 15, pp. 1657–1666.

Zadpoor, A. (2015). *Bone tissue regeneration: The role of scaffold geometry.* Biomaterials Science, 3(2), pp. 231–245.

Zhou, S., & Li, Q. (2008). *A variational level set method for the topology optimization of steady-state Navier-Stokes flow.* Journal of Computational Physics, 227(24), pp. 10178–10195.